Ore Geology Reviews 86 (2017) 117–129

Contents lists available at ScienceDirect

Ore Geology Reviews

journal homepage: www.elsevier.com/locate/oregeo

Fluid origin and migration of the Huangshaping W–Mo polymetallic deposit, South China: Geochemistry and $^{40}Ar/^{39}Ar$ geochronology of hydrothermal K-feldspars

Huan Li [a,*], Kotaro Yonezu [b], Koichiro Watanabe [b], Thomas Tindell [b]

[a] Department of Resources Science and Engineering, Faculty of Earth Resources, China University of Geosciences, Wuhan 430074, China
[b] Department of Earth Resources Engineering, Faculty of Engineering, Kyushu University, Fukuoka 819-0395, Japan

ARTICLE INFO

Article history:
Received 18 June 2016
Received in revised form 2 February 2017
Accepted 6 February 2017
Available online 9 February 2017

Keywords:
Hydrothermal K-feldspar
$^{40}Ar/^{39}Ar$ geochronology
Fluid migration
Mineralization rate
Huangshaping

ABSTRACT

The Huangshaping deposit is a world-class W–Mo–Pb–Zn–Cu polymetallic deposit that formed during the Jurassic magmatic event in the central Nanling region, South China. In order to reveal the three-dimensional development of mineralization and alteration in this complicated fluid-rock system, four typical hydrothermal K-feldspar samples were collected from potassic alteration zones at different elevation levels around main W–Mo ore bodies, followed by precise trace element analysis and $^{40}Ar/^{39}Ar$ dating. The results show that these K-feldspars have a pronounced lanthanide tetrad effect with high contents of Ga, Ta, Nb, U, Y and HREE but low concentrations of Ba, Sr, Eu and Zr, suggesting a hydrothermal origin. Additionally, correlation between the Ca/Cl/K ratios and the apparent ages suggest that metasomatic fluids played an important role in the formation of the hydrothermal K-feldspars. The plateau $^{40}Ar/^{39}Ar$ ages which represent the timing of potassic alteration vary from 152.9 ± 0.5 to 154.3 ± 0.6 Ma, spatially showing younger trends from north to south and from shallow to deep. These dates correspond to the previous published molybdenite Re–Os data variations in different elevation levels, which record the mineralization event with relatively older ages ranging from 153.8 to 159.4 Ma. Combined with the spatial relation analysis among samples, the fluid migration rates associated with the mineralization and alteration are calculated at 10–100 m Ma^{-1}. Thus, we propose a fluid downward migration model for the Huangshaping polymetallic deposit.

1. Introduction

Fluid flow and migration mechanisms in hydrothermal ore deposits draw great attention in economic geology due to their complicated processes (Boiron et al., 2001; Chung and Mungall, 2009; Tan et al., 2015). Channel way, direction and driving force of fluid migration are important components in ore genesis research. However, identifying detailed mineralization and alteration processes in the geologic record can be challenging, in part because of limited preservation of the earlier events and single dating approach in the complicated metallogenic system. In places where multiple dating methods are used, the rates and durations of mineralization and alteration can be determined and used to understand the ore genetic mechanisms (Deckart et al., 2005; Harris et al., 2008). Fluid-rock interaction features and alteration assemblages resulting from local chemical and/or thermal gradients may yield reliable information about their genesis and timing by dating isotopic reference minerals (Brockamp and Clauer, 2013). Additionally, laser probe $^{40}Ar/^{39}Ar$ analysis is also a powerful tool for extracting age information from hydrothermal minerals as a means to investigating fluid flow events (Sherlock et al., 2005). The recognition of ore deposits with fluids coming from deep and precipitating in a shallow environment has been widely advocated by geologists, while fluid downward migration and deposition are rarely reported.

Alkali feldspars are abundant in the continental crust, and being rich in K they are employed widely for radiometric dating by the K/Ar or $^{40}Ar/^{39}Ar$ methods to constrain the thermal history of rocks between temperatures of 150–500 °C (e.g., Warnock and Zeitler, 1998; Reddy et al., 1999, 2001; Flude et al., 2013; Lindsay et al., 2014). Wall rocks of ore deposits are often hydrothermally altered; and potassic alteration in some magmatic-hydrothermal deposits is commonly observed (e.g., Brockamp and Clauer, 2013). Potassium feldspar, an important indicator of a potassic alteration,

* Corresponding author at: Department of Resources Science and Engineering, Faculty of Earth Resources, China University of Geosciences, No. 388 Lumo Road, Wuhan 430074, China.
E-mail address: lihuan@cug.edu.cn (H. Li).

http://dx.doi.org/10.1016/j.oregeorev.2017.02.005
0169-1368/

occurs mainly in potassic alteration zones and is intensively employed to determine the mineralization ages of hydrothermal ore deposits (e.g., Reynolds et al., 1998; Wang et al., 2004; Zhu et al., 2015).

The Huangshaping W–Mo–Pb–Zn–Cu polymetallic deposit, located in the southern part of Hunan Province, South China, is hosted in Carboniferous sedimentary rocks around small plugs of Jurassic felsic porphyries. It is a representative skarn type deposit genetically related to Jurassic magmatism, with large metal concentrations. Since its commissioning in 1967, the total metal reserves have been proven up to 152.9 kt WO_3, 43.2 kt Mo, 761.3 kt Pb, 1529.1 kt Zn and 18.8 Mt Fe_3O_4, with average grades of 0.2%, 0.06%, 3.55%, 7.13% and 15.38%, respectively. Meanwhile, the total metal reserves of Cu, Sn and Bi have been recently estimated at 193.9 kt, 25.9 kt and 11.9 kt, respectively. Previous geochemical studies on mineralization-related porphyries and ores have been intensively carried out, indicating a complex magmatic and metallogenic process (e.g., Yao et al., 2005; Ma et al., 2007; Lei et al., 2010; Li et al., 2014a,b; Ding et al., 2016a,b). Although much geological research has been carried out for the Huangshaping deposit, accumulating a wealth of informative data, diverse results have also drawn some contradictory conclusions, which are both puzzling and intriguing. Thus, ore genesis remains a matter of controversy and new approaches are needed to constrain its mineralization and alteration processes. In this study, we carried out trace element analysis and $^{40}Ar/^{39}Ar$ dating for the hydrothermal K-feldspars of the mineralized porphyries, to refine our understanding of fluid evolutionary processes and fluid–rock interactions. Combined with previous published molybdenite Re–Os data, we propose a fluid downward migration model for the Huangshaping polymetallic deposit, aiming to shed some new insights into the principle ore-forming processes of skarn type hydrothermal ore deposits.

2. Regional and deposit geology

The Huangshaping polymetallic deposit is located in Chenzhou area, South Hunan (Fig. 1a). South Hunan is the most important component of the Nanling metallogenic belt in South China, which exhibits complex geologic conditions and rich mineral resources (Yao et al., 2007; Hu and Zhou, 2012). The Nanling region experienced complex tectonic movements at different stages and varying degrees, accompanied by igneous activity. The Jurassic magmatic activity played the most important role in the formation of granitic composites and mineral resources. It is characterized by multiple stages of intrusion which are associated with many polymetallic ore deposits (Mao et al., 2007). Recently, it is believed that the intensive Jurassic magmatism in this region occurred in an intraplate rift-related environment (Li et al., 2014a,b).

The exposed sedimentary rocks in the Huangshaping area are dominantly neritic marine sediments that can be subdivided into a number of different units (Fig. 1b). The Upper Devonian Xikuangshan Formation consists of thickly bedded limestones interbedded with chert at the lower part and calcareous sandstone at the upper part. The Lower Carboniferous is a set of sedimentary formations composed by interlayered littoral-neritic facies carbonate rocks and terrigenous clastic rocks. The lithologic units from bottom to top are composed of dolomitic limestone intercalated with argillaceous limestone and sandstone, medium bedded massive limestone, bioclastic limestone, sandstone interbedded with limy shale, and dolomite (Yao et al., 2007; Ding et al., 2016a; Li et al., 2016).

The granitoids associated with the Huangshaping deposit include quartz porphyry, granophyre and granite porphyry. These hypabyssal intrusions were laterally dissected by three normal faults (F_0, F_6 and F_9) (Fig. 1b) and longitudinally controlled by two thrust faults (F_1 and F_2) and an overturned anticline (Fig. 2a). The quartz porphyry intrusions form the Baoling and Guanyindazuo mountains, showing funnel-like shapes. The concealed granophyre bodies are in fault contact (some parts are in direct contact) with the quartz porphyry, appearing in the footwall of the fault F_1 (Fig. 2b). The granite porphyry bodies, also found underground, are intruded between F_1 and F_2 and located in the southeast portion of the mine. They mainly appear in the hanging wall of the F_1 fault and show no clear interspersed relations with other granitoids. Previous zircon U–Pb dating yielded ages ranging from 180 Ma to 155 Ma for these fresh porphyries (Lei et al., 2010; Quan et al., 2012; Li et al., 2014a; Ding et al., 2016b), and a general

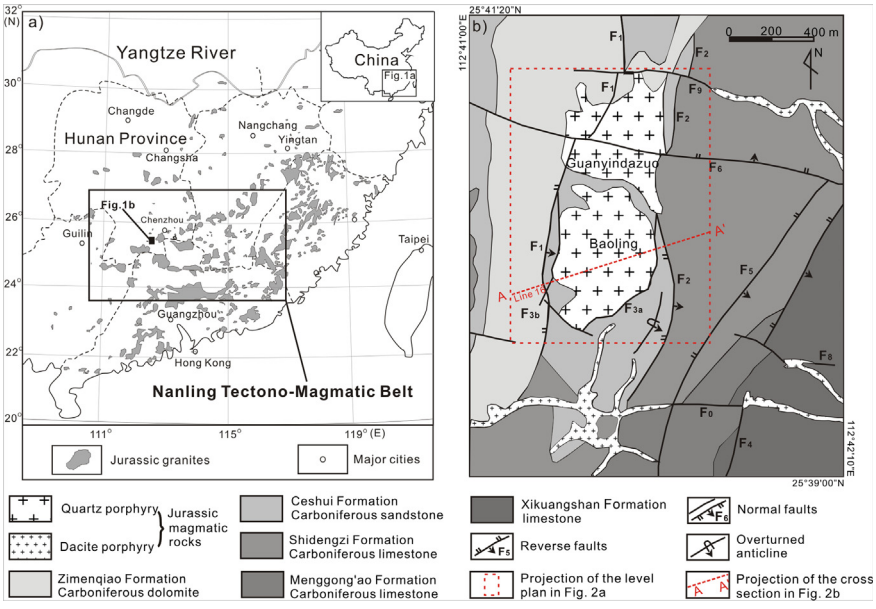

Fig. 1. (a) Simplified map showing the distribution of the Jurassic granites in South China (modified from Li et al. (2009)), and (b) Geological sketch map of the Huangshaping polymetallic deposit (modified from Yao et al. (2007)). The granophyre and the granite porphyry are not exposed on the surface. A level plan and cross section that display these two types of rock are shown in Fig. 2.

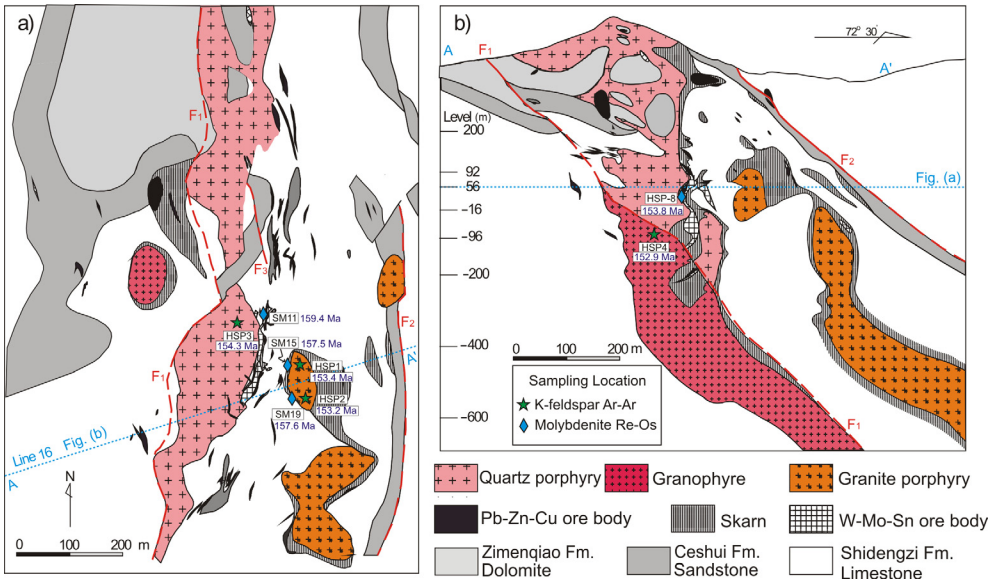

Fig. 2. Spatial relationship of various rock bodies from the Huangshaping polymetallic deposit (after Li et al., 2014a,b). (a) Level plan of 56-m elevation; (b) Cross section of Line 16.

intrusive sequence is acknowledged to be quartz porphyry → granophyre → granite porphyry (Li et al., 2014b).

The fresh granitoids in the Huangshaping deposit are gray to dark gray in color (Fig. 3a–c) but have distinct textures and mineral assemblages (Fig. 3d–f). The fresh quartz porphyry has a porphyritic texture (Fig. 3a) with quartz, K-feldspar, plagioclase and a small amount of biotite and hornblende as phenocrysts. The euhedral–subhedral K-feldspar consists of orthoclase, microcline and occasionally sanidine, characterized by irregular elongated secondary mineral strips, filling along its long axis (Fig. 3d). The fresh granophyre has a massive structure (Fig. 3b) and mainly consists of quartz, K-feldspar and plagioclase. The pristine K-feldspar is 0.05–0.1 mm in size and orthoclase–microcline in composition, with a euhedral–subhedral form (Fig. 3e). The fresh granite porphyry is porphyritic (Fig. 3c) and composed of quartz, K-feldspar, plagioclase and biotite as its major minerals. The fresh K-feldspar is 0.2–0.6 mm in size, with Carlsbad twin crystals (Fig. 3f).

All of the porphyries were partially modified by potassic and skarn alteration, present within the porphyries adjacent to the skarn (Fig. 3g–i). The mineral assemblages in the potassic altered quartz porphyry mainly include recrystallized quartz, K-feldspar and few plagioclases, with fine secondary minerals filling within these major phenocrysts (Fig. 3j). The hydrothermal K-feldspar phenocrysts of the altered quartz porphyry are mainly orthoclase, showing angular euhedral crystals and sometimes forming Carlsbad twin crystals, with albite exsolution within the crystals. In addition, plagioclase in the altered quartz porphyry was intensively modified by hydrothermal fluid, showing argillic alteration under the microscope (Fig. 3j). The potassic altered granophyre is predominantly recrystallized orthoclase and quartz. The orthoclase is characterized by rectangular tabular form, intergrown with myrmekitic quartz, and forming a granophyric and pegmatophyric texture (Fig. 3k). The mineralized granite porphyry shows a porphyritic or glomerophyric texture, mainly with perthite and quartz as its major minerals. The perthitic alkali feldspars are 0.2–0.4 mm in size and composed of albite lamellae as exsolution and microcline as its matrix (Fig. 3l).

Mineralization in the Huangshaping deposit can be divided into two stages, the earlier skarn stage and the later quartz-sulfide stage. The skarn type W–Mo polymetallic mineralization mainly occurs at the contact zones between the porphyries and limestone, with skarns preferentially developed around the granite porphyry. The skarn alteration is zoned from the granite porphyry and outwards to the distal limestone, with potassic alteration present within the granite porphyry adjacent to the skarn. The proximal skarn consists of garnet, diopside, chlorite, epidote and fluorite adjacent to the potassic-altered granite porphyry (Fig. 4a). Scheelite and molybdenite are commonly disseminated within the garnet–diopside skarn (Fig. 4b, c). The garnet–diopside zone is followed by the tremolite–actinolite skarn zone, which hosts tremolite, actinolite and calcite veins (Fig. 4d). The main polymetallic ore bodies are lenticular or quasi-lamellar in shape, located in the skarn between the quartz porphyry and the granite porphyry at 56 m elevation level (Fig. 2), extending into the fracture zones between the quartz porphyry and the granophyre at −96 m elevation level. The ore minerals in the skarn ores are magnetite (Fig. 4e, f), molybdenite (Fig. 4g), scheelite, bismuthinite and cassiterite. The quartz-sulfide stage Pb–Zn ore bodies are generally present as veins within the limestone, with galena, sphalerite and chalcopyrite as their major ore minerals (Fig. 4h, i). Based on our field investigation and microscopy observations and combined with previous research (Li et al., 2016; Ding et al., 2016a), the mineral paragenetic sequence for the two stages of mineralization in the Huangshaping deposit is shown in Fig. 5.

3. Sampling, analytical techniques and data processing process

Four typical hydrothermally altered and mineralized granitic porphyry samples were collected from different elevations in the underground tunnels around the main W–Mo polymetallic ore body of the Huangshaping Mine (Fig. 2). Samples HSP1, HSP2 and HSP3 were collected at the 56 m level (Fig. 2a), and sample HSP4 from the −96 m level (Fig. 2b). Consequently, four sets of hydrothermal K-feldspar samples, HSP1 and HSP2 from the granite porphyry, HSP3 from the quartz porphyry and HSP4 from the granophyre were separated. Potassium feldspar preparation was conducted in Kyushu University, where the samples were crushed, sieved, and separated by heavy liquid suspension in sodium polytungstate and followed by hand-picking under a binocular microscope, ensuring that the resulting sample was pure K-feldspar. The pure mineral extracts were then cleaned in de-ionized water

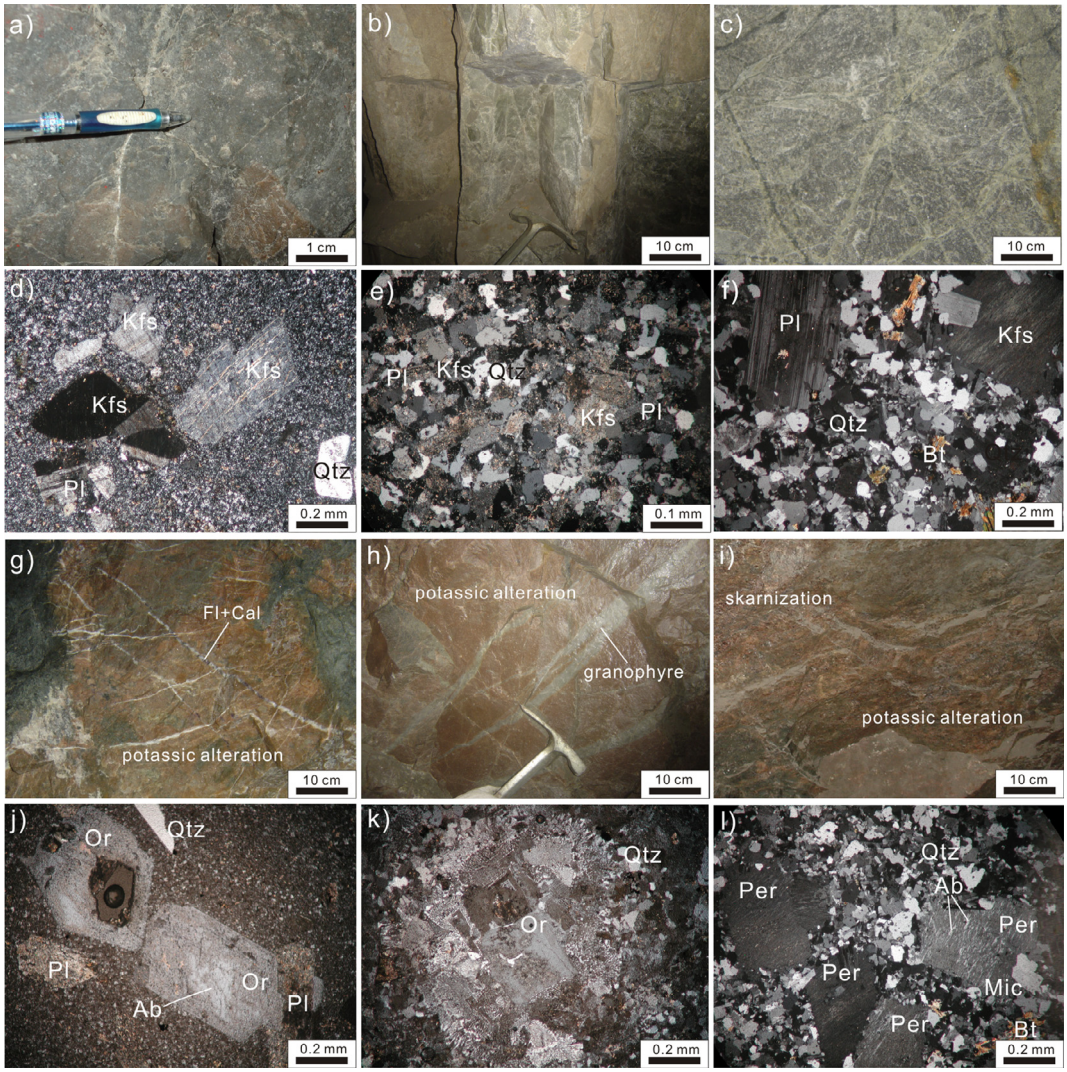

Fig. 3. Field occurrences (a–c, h–i) and photomicrographs (d–f, i–l) of the fresh and altered granitic porphyries from the Huangshaping polymetallic deposit. Left column (a, d, g, j): quartz porphyry; central column (b, e, h, k): granophyre; right column (c, f, i, l): granite porphyry. Cal: calcite; Fl: fluorite; Kfs: K-feldspar; Qtz: quartz; Bt: biotite. Or: orthoclase; Mic: microcline; Per: perthite; Ab: albite.

and acetone with an ultrasonic bath to remove any surface contamination. The procedure was repeated several times until the solution was clear. The K-feldspar separates were then powdered to 200-mesh using a vibration agate mill and were checked by X-ray diffraction with purities of better than 99%. The separated hydrothermal K-feldspars are orthoclase for quarz porphyry and granophyre whereas perthitic microcline for granite porphyry.

The separated K-feldspars were then analyzed for trace element compositions at ALS Laboratory, Canada. A prepared sample (0.2 g) was added to lithium borate flux (0.9 g), mixed well and fused in a furnace at 1000 °C. The resulting melt was then cooled and dissolved in 100 mL of 4% HNO_3/2% HCl solution. This solution was then analyzed by ICP-MS. Standard sample JG-2 was also used to monitor the reliability of analytical results, and the precision for most trace elements was better than 5%. The analytical results are presented in Table 1.

Potassium feldspars with grain size ranging from 180 to 250 μm were chosen for $^{40}Ar/^{39}Ar$ dating. Step-heating analyses follow the procedure outlined in Chew et al. (2008) and Kirkland et al. (2008). Potassium feldspar samples were irradiated at the NRG-Pattern HFR RADEO facility in the Netherlands. The step-heating analyses were performed at the $^{40}Ar/^{39}Ar$ Geochronology Laboratory, Department of Geology, Lund University, Sweden. Samples were step-heated using a defocused 50 W CO_2 laser and analyzed using a Micromass 5400 spectrometer with a Faraday and electron multiplier. The results were computed in plateau, total fusion and inverse isochron ages. The plateau age is the weighted mean of sequential concordant step ages that generally make up more than 50% of the released ^{39}Ar. The total fusion age (integrated age) is calculated by adding all step compositions to obtain a single age of total Ar gas released. The inverse isochron age are calculated from the slopes of the best fitting line to the Ar-isotopic computations of gas reduced during the temperature steps that make up the plateau age. Age results are shown in Table 2.

The previous published Re–Os dating results of molybdenite from the Huangshaping polymatallic deposit were systematically collected (Table 3), with the specific sampling locations shown in Fig. 2.

4. Results

4.1. Trace elements of hydrothermal K-feldspars

The rare earth element compositions of the K-feldspars show similar characteristics, though some variations may be

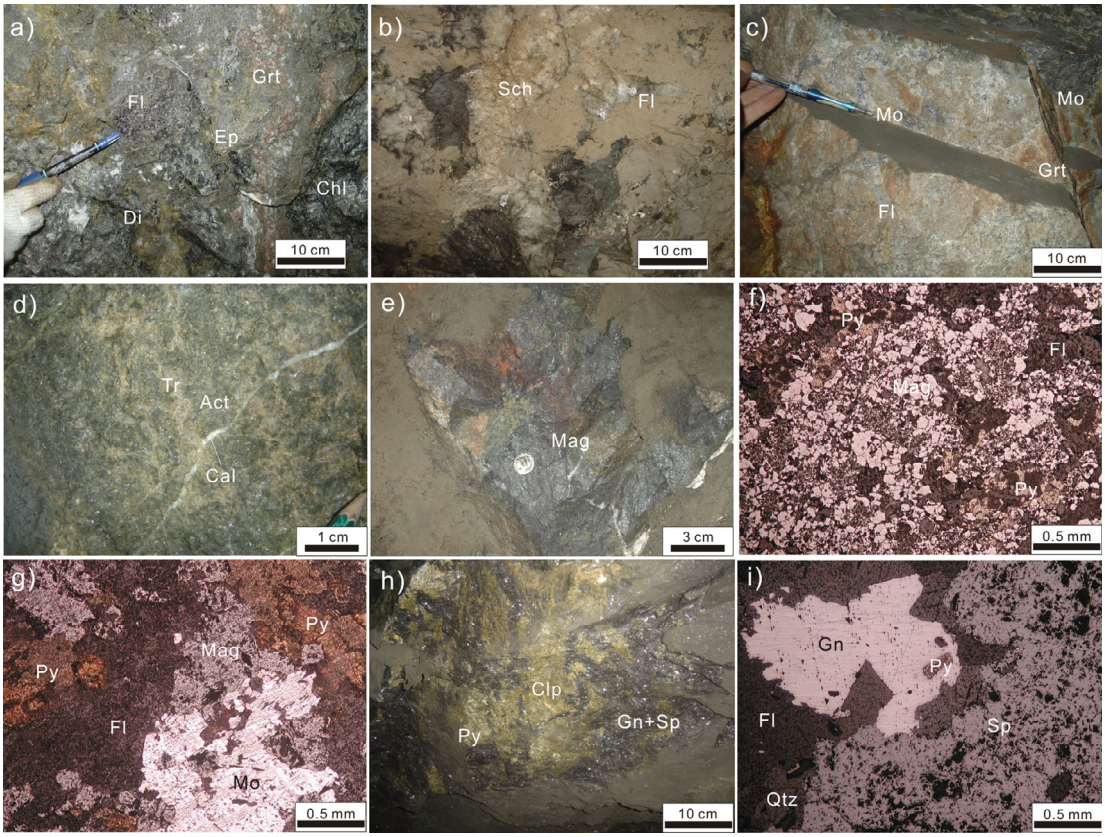

Fig. 4. Outcrop and photomicrographs of different types of skarn and mineralized ores in the Huangshaping polymetallic deposit. (a) garnet–diopside skarn; (b) W mineralization associated with the garnet–diopside skarn; (c) Mo mineralization associated with the garnet–diopside skarn; (d) tremolite–actinolite skarn; (e) magnetite mineralization associated with the tremolite–actinolite skarn; (f) microscopic characteristics of magnetite ore; (g) microscopy features of Mo-polymetallic ore; (h) quartz-sulfide stage Pb–Zn mineralization. (i) microscopic characteristics of Pb–Zn ore. Grt: garnet; Di: diopside; Ep: epidote; Chi: Chlorite; Fl: fluorite; Sch: scheelite; Mo: molybdenite; Tr: tremolite, Act: actinolite; Cal: calcite; Mag: magnetite; Cp: chalcopyrite, Sp: sphalerite; Py: pyrite.

distinguished. Sample HSP3 from the altered quartz porphyry has the lowest REE concentration and a flat pattern, with a LREE/HREE value of 1.96 (Fig. 6a). In contrast, sample HSP4 from the altered granophyre shows an obvious fractionation of LREE and HREE with a higher LREE/HREE value of 3.73. Both these two types of K-feldspar have similar Eu negative anomalies, with the δEu values of 0.05. On the other hand, the K-feldspar samples HSP1 and HSP2 from the mineralized granite porphyry are characterized by high concentrations of total REE and most pronounced negative Eu anomalies. They are more enriched in HREE, with LREE/HREE ratios ranging from 1.31 to 1.69. Furthermore, all of the K-feldspars show pronounced lanthanide tetrad effect on the REE patterns, with an order of increasing degree from the quartz porphyry to the granophyre and then to the granite porphyry. All of this indicates that these K-feldspars are hydrothermal in origin, and the K-feldspar samples from the mineralized granite porphyry underwent heavier fluid-feldspar interaction under a higher temperature.

The K-feldspars from the different types of mineralized granitoids also vary apparently in the concentrations of some trace elements (Fig. 6b). The K-feldspar samples HSP3 and HSP4 from the altered quartz porphyry and granophyre have similar trace element contents, whereas the K-feldspars HSP1 and HSP2 from the mineralized granite porphyry vary in several element compositions and show distinct characteristics. Compared to HSP3 and HSP4, the K-feldspars HSP1 and HSP2 have lower concentrations of Ba, Sr and Zr whereas higher contents of Ga, Ta, Nb, U and Y. This may also imply that the K-feldspars from the mineralized granite porphyry experienced more pronounced fluid metasomatism.

4.2. $^{40}Ar/^{39}Ar$ geochronology of hydrothermal K-feldspars

The $^{40}Ar/^{39}Ar$ plateau ages of the hydrothermal K-feldspars from the potassic alteration zone at the Huangshaping deposit range from 152.9 ± 0.5 to 154.3 ± 0.6 Ma; and the inverse isochron ages range from 153.5 ± 0.8 to 154.8 ± 0.8 Ma, correspondingly (Fig. 7). The normal Ca/K and Cl/K values range from 0.007 to 21.56 and between 0.001 and 1.263, respectively (Table 2). The small variations between the plateau age and the inverse isochron age of each sample indicate that these $^{40}Ar/^{39}Ar$ dating results are reliable. This is further proved by their initial $^{40}Ar/^{36}Ar$ ratios calculated by inverse isochron age diagrams, which range from 239 ± 20 to 283 ± 8 and are slightly lower but consistent with that of modern atmosphere (298, Lee et al., 2006; Pujol, 2013). This indicates no excess Ar was contained in these K-feldspar samples. Additionally, the integrated ages calculated on spectrum diagrams of these samples range from 152.3 ± 0.6 to 153.7 ± 0.7 Ma, which are also consistent with their plateau and isochron ages, respectively. The relatively flat step-heating age spectra and narrowed apparent age spans (small age gradients) indicate that these K-feldspars are hydrothermal in origin and did not suffer evident modification after the mineralization-related hydrothermal event; the K–Ar system has been well preserved after its formation; and the plateau ages can represent the alteration ages. Thus, the ages of the hydrothermal K-feldspars from the Huangshaping polymetallic deposit are determined at 153.4 ± 0.5 Ma (MSWD = 0.86), 153.2 ± 0.5 Ma (MSWD = 1.31), 154.3 ± 0.6 Ma (MSWD = 1.94) and 152.9 ± 0.5 Ma (MSWD = 1.51) for sample HSP1, HSP2, HSP3 and HSP4, respectively. Referring to the sampling location, clear

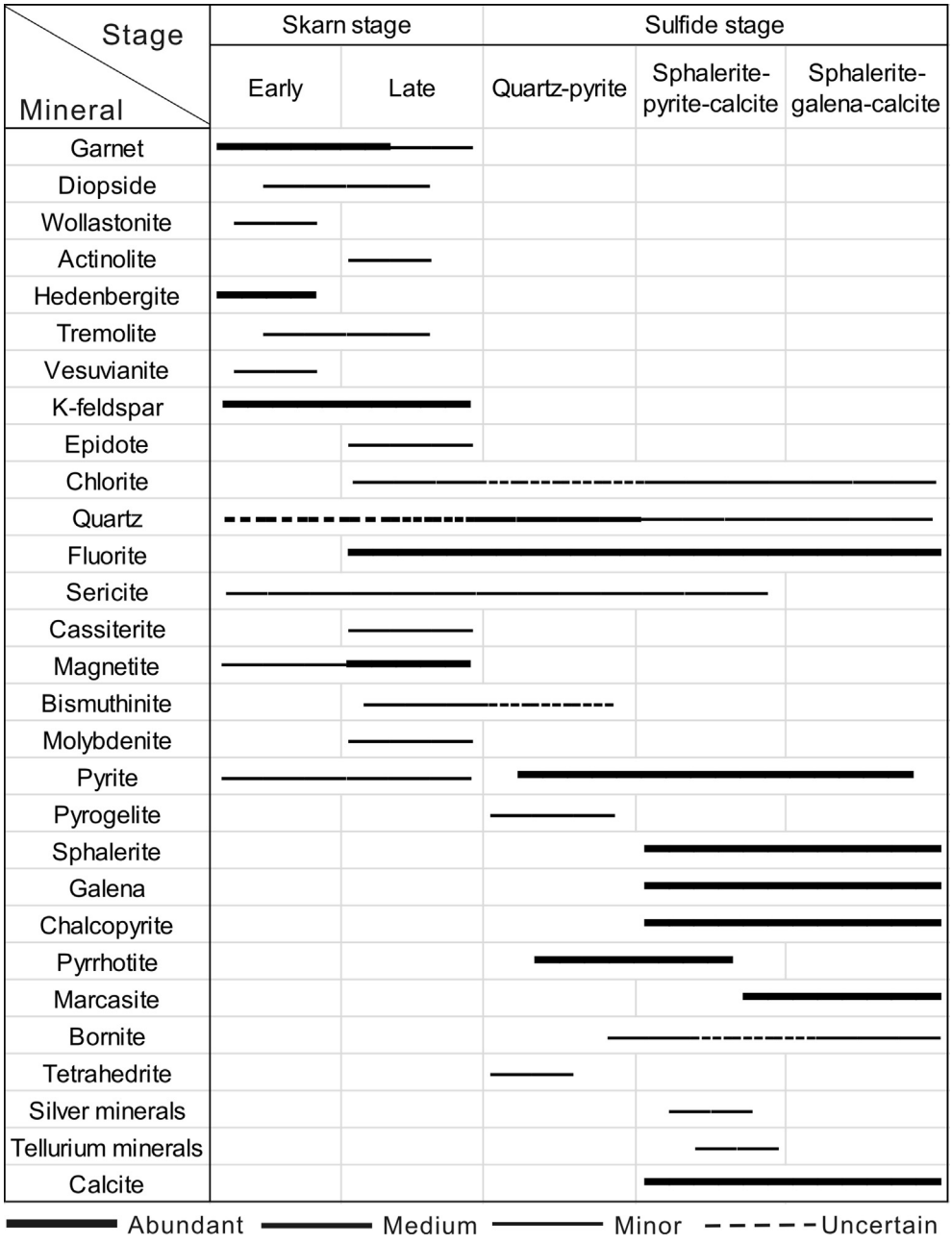

Fig. 5. Mineral paragenetic sequence for the two stages of mineralization in the Huangshaping polymetallic deposit.

younging age trends can be seen both from north to south at 56 m elevation level and from shallow (56 m elevation level) to deep (−96 m elevation level) (Fig. 2).

4.3. Re–Os geochronology of molybdenites

The previous published molybdenite isochron Re–Os dating results of the Huangshaping polymetallic deposit also vary both vertically and horizontally. At the 56 m elevation level, the mineralization ages change from 159.4 ± 3.3 Ma to 157.5 ± 2.1 Ma and 157.6 ± 2.3 Ma from north to south in the main W–Mo polymetallic ore bodies (Lei et al., 2010), and then to 153.8 ± 4.8 Ma at 20 m elevation level (Ma et al., 2007). The other published molybdenite Re–Os age dates fall into this time span, ranging from 154.8 ± 1.9 Ma (isochron age, Yao et al., 2007) to 154.2 ± 2.2 Ma and 153.9 ± 1.7 Ma (model ages, Mao et al., 2007).

5. Discussion

5.1. Genesis of the hydrothermal K-feldspars in the Huangshaping deposit

The $^{40}Ar/^{39}Ar$ dating of K-feldspars and fluid modeling need complete understanding of the genesis of microtextures in hydrothermal feldspars (McLaren et al., 2007). The different microtextures in the hydrothermal K-feldspars from the quartz granite, granophyre and granite porphyry may indicate distinct hydrothermal process and temperature conditions. The perthitic textures shown in the K-feldspars from the mineralized granite porphyry may indicate that they have formed at moderate to high temperature conditions during the sub-solidus phase (Pandit, 2015). A small amount of locally exsolved magmatic fluid may have been involved in the development of the perthitic texture in alkali

Table 1
Trace element compositions of hydrothermal K-feldspars from the Huangshaping polymetallic deposit.

Sample No.	HSP1	HSP2	HSP3	HSP4
Host granite	*Granite porphyry*		*Quartz porphyry*	*Granophyre*
La	8.6	11.8	5.6	16.8
Ce	22.3	29.6	15	39.1
Pr	3.03	3.86	2.11	4.93
Nd	14.3	17.2	8.8	19.4
Sm	6.68	6.96	3.07	5.6
Eu	<0.03	<0.03	0.05	0.1
Gd	7.78	8.2	3.26	5.52
Tb	1.54	1.59	0.69	0.93
Dy	10.75	10.75	5.11	5.7
Ho	2.37	2.15	1.03	1.32
Er	7.67	7.25	3.25	3.84
Tm	1.26	1.2	0.51	0.6
Yb	9.1	8.62	3.36	4.47
Lu	1.44	1.27	0.5	0.66
ΣREE	96.84	110.47	52.34	108.97
LREE	54.93	69.44	34.63	85.93
HREE	41.91	41.03	17.71	23.04
LREE/HREE	1.31	1.69	1.96	3.73
La_N/Yb_N	0.64	0.93	1.13	2.54
δEu	0.01	0.01	0.05	0.05
δCe	1.02	1.03	1.02	1.01
Ba	5	5.8	51.3	33
Cr	<10	<10	<10	<10
Cs	5.07	16.5	4.68	6.29
Ga	26.1	25.2	19.2	18.5
Hf	7.1	5.7	5.3	4.6
Nb	66.6	56.2	39.7	34.7
Rb	598	992	675	597
Sn	4	16	17	13
Sr	3.2	5.7	36.4	41.1
Ta	13.6	8.7	4	3.4
Th	31.8	29.7	31.8	30.9
Tl	2.6	3.5	2.9	2.7
U	19.75	18.05	12.35	10.6
V	<5	<5	<5	<5
W	1765	133	143	167
Y	73	75.2	29.3	36.1
Zr	94	75	112	116

feldspar at ~400 °C (Liu, 2002). The coarsened microperthitic textures in the alkali feldspar imply a metasomatic origin and significant feldspar–water interaction. Formation of microperthite in the mineralized granite porphyry can be explained by the replacement reaction mechanism (Na–K exchange) between K-feldspar and plagioclase during a magmatic-hydrothermal transition phase under a rapid cooling condition at upper or shallow levels in the continental crust (Pandit, 2015). During this process, plagioclase can be decomposed under the influence of H_2O fluids, forming albite, quartz and other minerals, deriving the perthite (Leichmann et al., 2009). The granite porphyry may have undergone extensive subsolidus re-equilibration, changing the original magmatic mineralogy. The replacement reactions may be due to sequential fluid infiltration events (Plümper and Putnis, 2009). In contrast, low to moderate temperature conditions could be favored for the formation of orthoclase in the altered granophyre and quartz porphyry. The myrmekites in the orthoclase and recrystallized quartz from the altered granophyre may suggest that meteoric-derived water plays an important role in the further development of alkali feldspar exsolution texture mainly via dissolution–reprecipitation. During this process, the original plagioclase was metasomatised by the hydrothermal fluid, forming the orthoclase with the exsolution of albite. The residual plagioclase in the altered quartz porphyry also indicates weakened fluid modification and decreased temperature for the crystallization of the orthoclase. During the K-feldspar alteration, elements such as Al, Ca, Na, Fe and Mg of original minerals were taken out, reacting with F and CO_2 in the fluid and then forming the fluorite and calcite in the potassic alteration zone (Fig. 3g). In summary, the sub-solidus alteration and microtextural development of the hydrothermal K-feldspars began with the intrusion of the granite porphyry at a relatively high temperature; and magmatic fluids which underwent intense feldspar–water metasomatism dominated the perthite crystallization process. This was followed by increasing involvement of meteoric water, resulting in the formation of orthoclase in the altered granophyre and quartz porphyry under a relatively lower temperature condition.

5.2. Geological and geochronological significances of the hydrothermal K-feldspars

The $^{40}Ar/^{39}Ar$ radiometric system in K-feldspar has closure temperatures of 150–350 °C (McDougall and Harrison, 1999) which is lower than that of the potassic alteration (Frank and Vaccaro, 2012); thus, the crystallization age of K-feldspars represent the minimum age of potassic alteration (Zhu et al., 2015). On the other hand, analysis of K-feldspar by the $^{40}Ar/^{39}Ar$ method can give information on the very latest perturbations in the area since K-feldspars have multiple, low closure temperatures (Streepey et al., 2002). The first few percent of total gas release yielded anomalously low ages (dominantly 140–150 Ma), which may be related to a small amount of argon loss after post-crystallization cooling, or may be ascribed to slight argon loss and atmospheric argon adsorption in the outer lattice of the minerals.

The preservation capacity of the argon isotopic system in different geological settings and processes may be significantly different

Table 2
$^{40}Ar/^{39}Ar$ step-heating data for hydrothermal K-feldspars from the Huangshaping polymetallic deposit.

Sample/run ID	Power (W)	Ca/K	Cl/K	$^{36}Ar/^{39}Ar$	$^{40*}Ar/^{39}Ar$	^{39}Ar (mol 10^{-14})	$\%^{39}Ar$ in step	Cum.$\%^{39}Ar$	% rad. $^{40}Ar^{*}$	Age (Ma)	±2σ
HSP1, Run ID# 2326-01 (J = 0.004709 ± 4.500000e−6)											
2326-01A	2.8	21.563	1.263	0.6676	-195.082	0.00	0.0	0.0	-7229.7	(4526.25)	7191.20
2326-01B	3.1	0.066	0.001	0.0238	17.921	0.49	9.3	9.3	71.8	146.17	0.76
2326-01C	3.4	-27.264	-0.476	-0.1912	87.459	0.00	0.0	9.2	270.1	622.22	102.10
2326-01D	3.7	3.202	-0.037	0.0300	10.744	0.01	0.1	9.3	55.1	89.04	35.19
•2326-01E	4.0	0.062	0.000	0.0025	18.882	2.22	41.9	51.2	96.3	153.67	0.34
•2326-01F	4.2	0.024	0.001	0.0035	18.856	0.89	16.8	67.9	94.8	153.47	0.37
•2326-01G	4.4	0.029	0.001	0.0044	18.810	1.16	21.9	89.8	93.6	153.11	0.38
•2326-01H	4.6	0.066	0.001	0.0059	18.856	0.32	6.1	95.9	91.6	153.48	0.59
•2326-01I	4.8	0.350	0.005	0.0036	19.105	0.04	0.7	96.6	94.8	155.41	3.24
•2326-01J	5.0	0.032	0.002	0.0058	18.799	0.13	2.5	99.1	91.6	153.02	1.02
•2326-01K	5.3	0.142	0.002	0.0085	18.268	0.05	0.9	100.0	88.0	148.88	2.47
2326-01L	5.6	0.601	0.006	0.1581	16.062	0.02	0.3	99.3	25.6	131.54	7.79
2326-01M	5.9	1.943	0.016	0.0118	18.778	0.01	0.3	99.6	84.6	152.86	8.23
2326-01N	6.2	3.426	0.046	0.3776	16.241	0.01	0.2	99.7	12.7	132.95	16.81
2326-01O	6.5	4.055	0.038	0.0541	11.342	0.01	0.1	99.9	41.7	93.87	16.70
2326-01P	7.0	-1.699	0.000	0.3965	23.542	0.01	0.1	100.0	16.7	189.67	25.60
2326-01Q	8.0	-5.386	-0.138	0.8763	20.192	0.00	0.0	100.0	7.2	163.87	71.39
Integ. Age=										152.8	0.5
(•) Plateau Age=							90.7			153.4	0.5
HSP2, Run ID# 2326-02 (J = 0.004709 ± 4.500000e-6)											
2326-02A	2.8	0.037	0.001	0.0731	17.150	0.10	2.0	2.0	44.3	140.11	2.00
2326-02B	3.1	-68.632	-1.547	0.4638	-91.422	0.00	0.0	2.0	-202.1	(1015.71)	1602.68
2326-02C	3.4	-0.451	-0.010	0.0035	20.196	0.02	0.3	2.4	95.0	163.90	6.40
•2326-02D	3.7	0.264	0.000	0.0027	18.742	1.82	37.4	39.4	95.9	152.58	0.40
•2326-02E	4.0	0.020	0.001	0.0029	18.903	1.20	24.6	64.0	95.7	153.84	0.38
•2326-02F	4.2	0.066	0.001	0.0054	18.824	0.52	10.6	74.6	92.2	153.22	0.55
•2326-02G	4.4	0.014	0.000	0.0048	18.800	0.69	14.2	88.8	93.0	153.04	0.53
•2326-02H	4.6	0.082	0.004	0.0062	18.601	0.03	0.6	89.3	91.0	151.48	4.30
•2326-02I	4.8	0.179	0.001	0.0057	19.120	0.05	1.0	90.3	91.9	155.53	2.38
2326-02J	5.0	0.076	0.001	0.0082	18.123	0.40	8.2	98.5	88.2	147.75	0.57
2326-02K	5.3	0.405	0.014	0.0094	18.158	0.04	0.8	99.3	86.8	148.02	3.03
2326-02L	5.6	0.894	0.009	0.0091	17.634	0.03	0.7	100.0	87.0	143.91	3.48
2326-02M	5.9	0.634	0.054	0.0130	16.438	0.01	0.1	99.4	81.2	134.50	14.47
2326-02N	6.2	1.711	0.025	0.0184	15.115	0.01	0.2	99.6	73.7	124.05	13.20
2326-02O	6.5	2.195	0.033	0.0431	9.094	0.01	0.1	99.7	41.8	75.65	18.52
2326-02P	7.0	0.129	-0.002	0.0128	17.371	0.01	0.3	100.0	82.1	141.85	8.01
2326-02Q	8.0	14.723	0.661	0.2283	-31.432	0.00	0.0	100.0	-87.8	(288.98)	247.79
Integ. Age=										152.3	0.6
(•) Plateau Age=							88.3			153.2	0.5
HSP3, Run ID# 2325-01 (J = 0.004709 ± 4.500000e−6)											
2325-01A	3.4	0.067	0.000	0.0081	18.615	2.86	17.1	17.1	88.6	151.59	0.42
2325-01B	3.7	-2.907	0.029	0.0012	18.269	0.01	0.0	17.1	97.6	148.88	23.58
2325-01C	4.4	0.406	0.019	0.0079	17.227	0.02	0.1	17.2	88.1	140.72	6.40
•2325-01D	4.7	0.130	0.000	0.0001	19.206	0.12	0.7	17.8	99.8	156.20	0.96
•2325-01E	5.0	0.114	0.000	0.0003	18.973	0.40	2.4	20.2	99.6	154.38	0.55
•2325-01F	6.0	0.139	0.001	0.0013	18.964	10.47	62.7	83.0	98.1	154.31	0.41
•2325-01G	7.0	0.049	0.002	0.0025	18.870	2.35	14.1	97.0	96.3	153.58	0.52
2325-01H	8.0	0.020	0.002	0.0078	18.516	0.50	3.0	100.0	89.0	150.82	0.66
Integ. Age=										153.7	0.7
(•) Plateau Age=							79.9			154.3	0.6
HSP4, Run ID# 2327-01 (J = 0.004709 ± 4.500000e−6)											
2327-01A	2.8	0.818	0.001	0.0516	17.549	0.76	5.8	5.8	53.5	143.25	0.79
•2327-01B	3.1	0.516	0.000	0.0019	18.844	1.44	11.0	16.8	97.2	153.38	0.30
•2327-01C	3.4	0.181	0.000	0.0006	18.773	1.75	13.4	30.1	99.1	152.83	0.45
•2327-01D	3.7	1.384	0.041	-0.0172	25.618	0.01	0.0	30.0	125.0	205.48	21.37
•2327-01E	4.0	0.488	-0.001	-0.0033	20.241	0.02	0.2	30.2	105.2	164.24	4.79
•2327-01F	4.2	0.049	0.000	0.0012	18.761	5.15	39.3	69.4	98.2	152.73	0.51
•2327-01G	4.4	0.075	0.000	0.0019	18.705	1.81	13.8	83.2	97.0	152.29	0.44
2327-01H	4.6	0.043	0.000	0.0020	19.000	1.05	8.0	91.2	97.0	154.60	0.36
2327-01I	4.8	0.007	0.000	0.0015	19.020	0.80	6.1	97.3	97.7	154.75	0.36
2327-01J	5.0	0.010	0.000	0.0021	19.039	0.35	2.7	100.0	96.9	154.90	0.59
2327-01K	5.3	0.621	-0.020	0.0014	19.238	0.01	0.1	99.7	98.0	156.45	15.33
2327-01L	5.6	-0.820	0.067	0.0010	19.900	0.00	0.0	99.8	98.5	161.60	23.83
2327-01M	5.9	-4.343	0.102	0.0111	15.505	0.00	0.0	99.8	81.9	127.14	38.48
2327-01N	6.2	-1.767	0.046	-0.0098	22.200	0.00	0.0	99.8	114.6	179.38	28.88
2327-01O	6.5	0.581	0.157	0.0245	11.737	0.00	0.0	99.8	61.9	97.06	45.14
2327-01P	7.0	2.568	0.040	0.0402	7.187	0.00	0.0	99.9	37.9	60.05	37.70
2327-01Q	8.0	0.243	-0.006	0.0004	19.389	0.02	0.1	100.0	99.4	157.62	5.70
Integ. Age=										152.5	0.6
(•) Plateau Age=							77.4			152.9	0.5

Data are corrected for machine blank, correction factors and $^{37}Ar/^{36}Ar$ post-irradiation decay.
(•) = Steps used in calculation of the plateau age.

Table 3
Previous published Re–Os dating results of molybdenite from the Huangshaping polymetallic deposit.

Sample No.	Location	Model age	Isochron age	References
SM11-1	Level 56 m	155.1 ± 2.5	159.4 ± 3.3	Lei et al. (2010)
SM11-2	Level 56 m	157.3 ± 2.4		
SM11-3	Level 56 m	163.9 ± 4.1		
SM11-4	Level 56 m	164.6 ± 6.8		
SM11-5	Level 56 m	155.4 ± 2.2		
SM11-6	Level 56 m	146.8 ± 6.1		
SM11-7	Level 56 m	157.6 ± 2.3		
SM15-1	Level 56 m	158.0 ± 2.7	157.5 ± 2.1	
SM15-2	Level 56 m	156.9 ± 2.2		
SM15-3	Level 56 m	155.0 ± 2.6		
SM15-4	Level 56 m	155.5 ± 2.2		
SM15-5	Level 56 m	157.1 ± 2.3		
SM15-6	Level 56 m	157.8 ± 2.3		
SM15-7	Level 56 m	156.2 ± 2.4		
SM19-1	Level 56 m	155.4 ± 2.6	157.6 ± 2.3	
SM19-2	Level 56 m	154.7 ± 2.9		
SM19-3	Level 56 m	156.9 ± 2.4		
SM19-4	Level 56 m	158.2 ± 2.3		
SM19-5	Level 56 m	157.1 ± 2.2		
SM19-6	Level 56 m	155.9 ± 2.3		
HSP-8-2	Level 20 m	154.3 ± 1.9	153.8 ± 4.8	Ma et al. (2007)
HSP-8-3	Level 20 m	155.5 ± 1.9		
HSP-8-5	Level 20 m	165.6 ± 2.2		
HSP-8-6	Level 20 m	161.0 ± 2.0		
H-6	Unknown	154.9 ± 3.0	154.8 ± 1.9	Yao et al. (2007)
H-46	Unknown	153.5 ± 3.2		
H-47	Unknown	156.9 ± 2.6		
H-48	Unknown	150.9 ± 2.6		
H-49	Unknown	156.2 ± 2.6		
H-59	Unknown	155.0 ± 3.9		
Unknown	Unknown	154.2 ± 2.2		Mao et al. (2007)
Unknown	Unknown	153.9 ± 1.7		

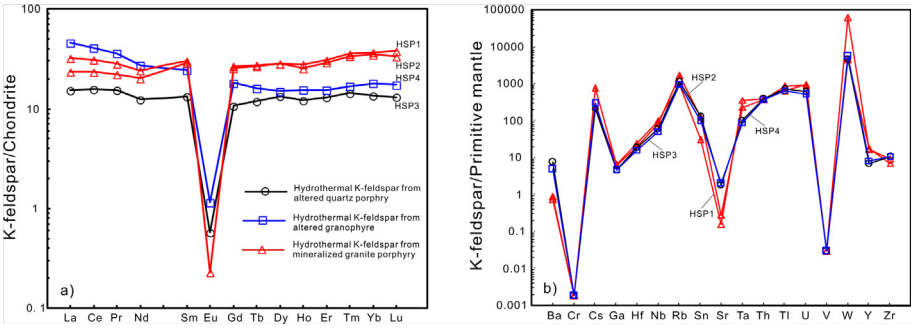

Fig. 6. (a) Chondrite-normalized REE patterns and (b) primitive mantle-normalized trace element patterns for hydrothermal K-feldspars from the Huangshaping polymetallic deposit. Normalized values for chondrite and primitive mantle are from Taylor and McClennan (1985), and Sun and McDonough (1989), respectively.

from each other, resulting in distinct age spectrums for K-feldspars (McLaren et al., 2007). The K-feldspars from plutonic rocks or metamorphic rocks often have complicated $^{40}Ar/^{39}Ar$ age spectrums, suggesting a long and complex thermal history (Warnock and Zeitler, 1998). In contract, hydrothermal K-feldspars usually yield flat age spectrums (Wilson et al., 2003). The homogeneous and flat $^{40}Ar/^{39}Ar$ age spectra of the K-feldspars from the Huangshaping deposit indicate that they are hydrothermal in origin and cooled down quickly and uniformly. The low initial $^{40}Ar/^{36}Ar$ ratios in the hydrothermal K-feldspars from the Huangshaping deposit imply that low level of atmospheric Ar was captured during the mineralization. This may indicate that the mineralization-related fluid is magmatic in origin, because high levels of atmospheric Ar may be attributed to connate meteoric fluids incorporated into basinal metamorphic fluids (Wilson et al., 2003). The present $^{40}Ar/^{39}Ar$ dating study of the K-feldspar associated with the W–Mo polymetallic mineralization defines the age of hydrothermal alteration, which occurred at ca. 154–153 Ma. This thermal event reflects a structurally channeled and relatively short-lived magmatic fluid pulse with temperatures >300 °C and overlays in space with emplacement of the Jurassic porphyries in the Huangshaping region.

The Ca/K and Cl/K ratios calculated from artificial Ar isotope production play an important role in determining mineral mixtures, fingerprinting their end-members and revealing hydrothermal fluid features (Esser et al., 1997; Solé et al., 2002; Sherlock et al., 2005). During irradiation, ^{37}Ar and ^{38}Ar are formed from Ca and Cl, respectively. Combined with the ^{39}Ar release data indicated by age spectra, it may exploit the full potential of the $^{40}Ar/^{39}Ar$ technique especially when the correlation between the Ca/Cl/K ratios and the $^{40}Ar^{*}/K$ ratio (i.e., the apparent step age) occurs (Chafe et al., 2014). For the K-feldspar samples from the Huangshaping deposit, the Ca/K and Cl/K values have a positive correlation (Fig. 8a). Moreover, the extremely high Ca/K and Cl/K values dominantly occur at

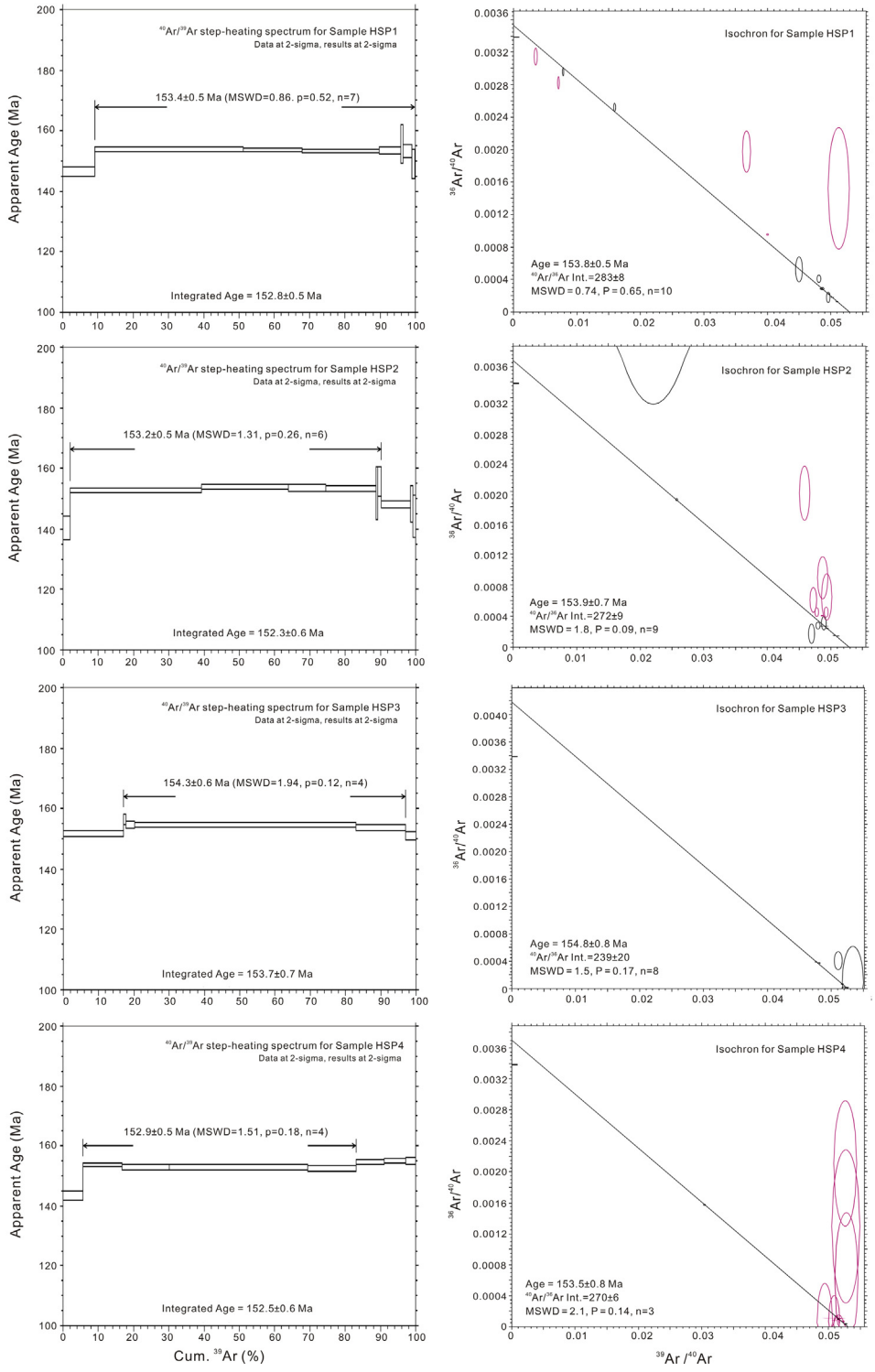

Fig. 7. $^{40}Ar/^{39}Ar$ step heating spectrums and inverse isochron ages of hydrothermal K-feldspar from the Huangshaping polymetallic deposit.

the first and last few heating steps (Table 2) and are negatively related to the apparent ages (Fig. 8b, c). These observations are evidence that finely inter-grown, Cl-rich alteration phases (e.g., sericite) most likely account for these steps, which often correspond to the lowest step ages. Furthermore, the Ca/K values of the K-feldspars from the Huangshaping deposit show more varied and higher ratios relative to Cl/K values, especially for the sample HSP1 and HSP2, which were hosted in the granite porphyry. This may suggest that metasomatic fluids derived from the intense skarnization, associated with the granite porphyry, played an important role in the formation of the hydrothermal K-feldspars. These secondary K-feldspar from the Huangshaping deposit may have record open-system fluid infiltration, patchy metasomatic alteration and retrograde replacement reactions.

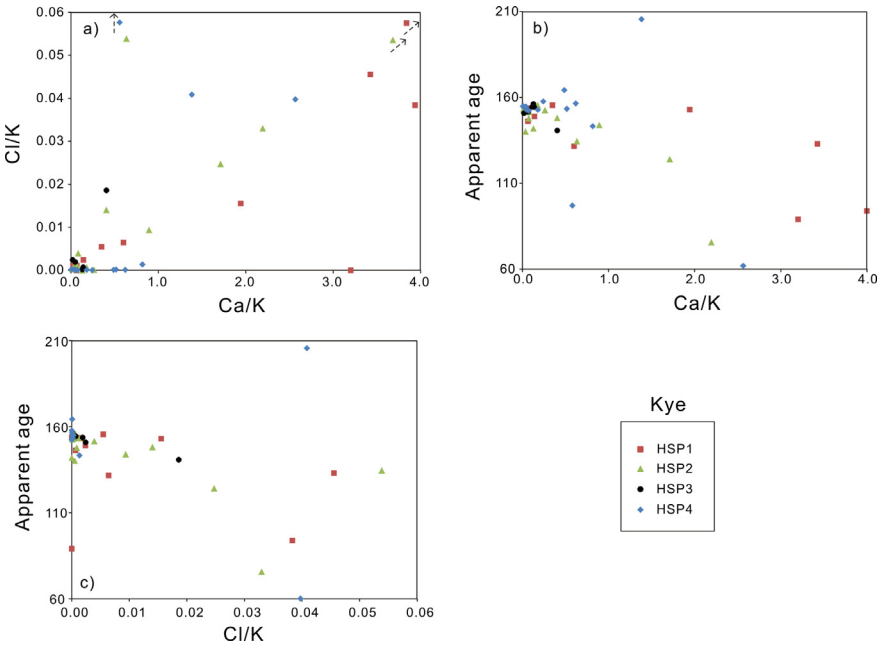

Fig. 8. Correlation diagrams of (a) Cl/K vs. Ca/K, (b) apparent age vs. Ca/K and (c) apparent age vs. Cl/K for hydrothermal K-feldspar from the Huangshaping polymetallic deposit.

5.3. Three-dimensional fluid migration model

The granite porphyry that contributed to the skarn type mineralization have been dated at ~160 Ma by previous zircon U–Pb geochronology (Yao et al., 2005; Li et al., 2014a; Ding et al., 2016b). The mineralization ages supported by the previous Re–Os dating and alteration ages yielded by the $^{40}Ar/^{39}Ar$ dating are younger than but close to 160 Ma. Thus, we can infer that the major W–Mo polymetallic mineralization occurred in the immediate aftermath of the intrusive granite porphyry. Based on this, a general sequence of fluid migration and precipitation can be drawn to reconstruct the mineralization and alteration processes. A high temperature, Cl-rich metasomatic fluid derived from the granite porphyry initiating at ~160 Ma. At 56 m elevation level, the fluid migrated along the N–S trending fractures close to the quartz porphyry. This initially precipitated at its northern end at 159.4 Ma and is recorded by sample SM11 (Fig. 2a). Horizontally, this was followed by a southward fluid flow, which is encountered at the location of SM15 at 157.5 Ma and SM19 at 157.6 Ma. This is accompanied by strong skarnization. The duration of mineralization can therefore be estimated at approximately ~2 Ma forming the ore bodies with a total horizontally length of around 200 m. However, it may have taken a longer time to alter the near-ore porphyries, which is estimated at 4 Ma at HSP3 and 3 Ma to reach HSP1 and HSP2 for the ore-accompanied fluid, with approximate ore–porphyry distances of 40 m and 30 m, respectively. Thus, at 56 m elevation level, the fluid migration rate and alteration rate can be estimated at 100 m Ma^{-1} from north to south inside the ore body and 10 m Ma^{-1} inside the country rocks from the center to periphery. Simultaneously, the fluid migrated vertically to a deeper elevation reaching the 20 m elevation level at 153.8 Ma (sample HSP-8). It then took about 3.8 Ma for the fluid to migrate a vertical distance of 36 m inside the main ore bodies. Consequently, the fluids downward migration rate is estimated at ~10 m Ma^{-1}. Towards the deeper levels, the mineralization becomes weakened, conversely the alteration considerably strengthened. Fluids passed through the at −96 m elevation level at 152.9 Ma (sample HSP4, Fig. 2b), with a fast water-rock interaction rate of around 100 m Ma^{-1}. Thus, a downward fluid migration model can be established for the Huangshaping polymetallic deposit (Fig. 9).

5.4. Mechanism of the fluid downward migration

In recent years, ore-fluid circulation models have been extensively developed, and fluid driving factors are mainly ascribed to gradients of pressure, thermal, buoyancy and gravity (e.g., Boiron et al., 2001; Zhu and Yang, 2006; Tan et al., 2015). In a long-lived hypabyssal mineral system, fluid movement is more likely to be driven by gravity and pressure rather than other factors (Relvas et al., 2006; Subias et al., 2015). The large variations of Re–Os and $^{40}Ar/^{39}Ar$ geochronological systems suggest a long polymetallic mineralization period in the Huangshaping deposit. Rapid fluid expulsion within deeper formations leads to a downwards-decreasing pressure gradient that subsequently draws down fluid from within overlying strata (Frazer et al., 2014). The downward impelling force associated with fluid-overpressure and gravity gradients in the closed system was stronger than the buoyancy force, resulting in the deep forward fluid. In compressional tectonic settings, fluid flow may be directed downward to a depth of tectonically induced neutral buoyancy (Connolly and Podladchikov, 2004). As long as the pressure gradient remains, fluids are capable of migrating distances of hundreds of meters vertically through geological bodies (Chung and Mungall, 2009). When the vertical height is great enough, the pressure gradient inside the dense phase may exceed the capillary force; and the immiscible phase is able to move down along vertically-oriented networks. Such a flow development may have important implications for the relative timing and distribution of a sequence of diagenetic products within the polymetallic system. Ore deposition resulted from fluid migration through a series of dense and regular sets of structures (veinlets and microfissures). During this process, gravity-driven fluids have interacted with the wall rocks, partially altering the

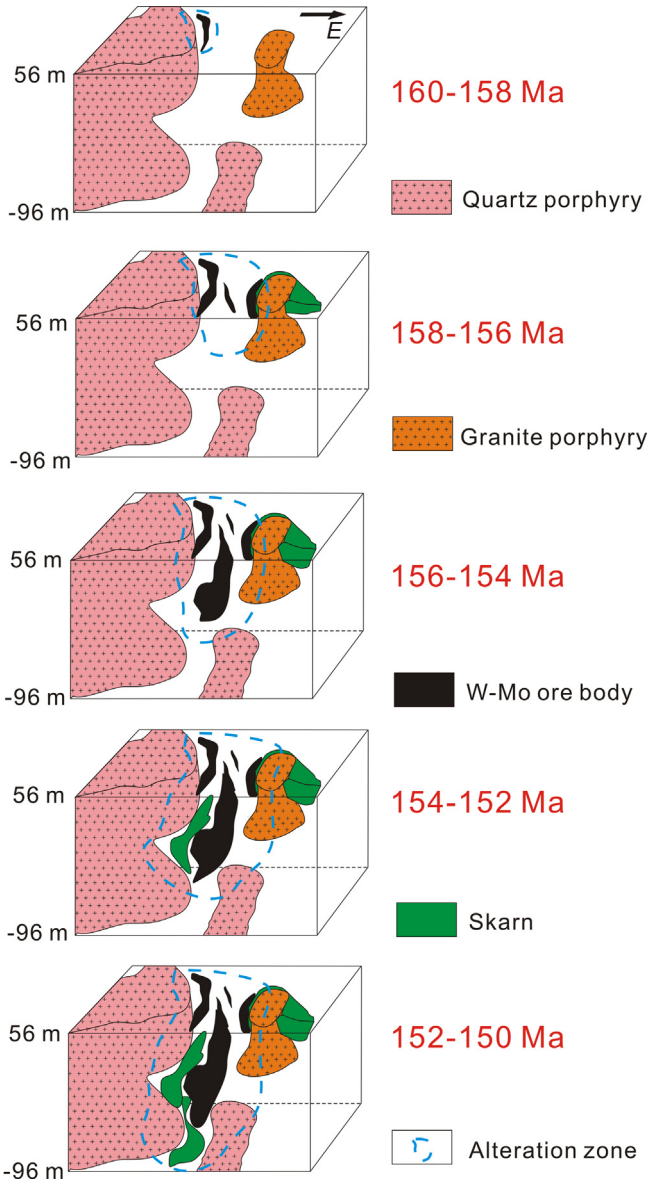

Fig. 9. A downward fluid migration model to illustrate the W–Mo mineralization and alteration processes in the Huangshaping polymetallic deposit.

magmatic K-feldspars into secondary K-feldspars, with strong skarnization. Ore body-scale geochronology reflects the passage of fluids through the rocks. Rock strata and structures allowed the ore-forming fluids to migrate vertically along the unconformity between the porphyries and limestone; this converged on the high elevation intrusive tip of the granite porphyry, then descending into the underlying strata along fractures. The fluid that circulated at the contact of the orebody was oxidizing, whereas the fluid circulating distally from it was more reduced. This may be due to the combination of water radiolysis and differential migration of H_2 and O_2 (Derome et al., 2003). The W–Mo polymetallic mineralization may occur preferentially in an oxidizing condition (Li et al., 2014b). This can be applied to explain the weakened and slowed trends for the mineralization whereas enhanced and accelerated advance of alteration from 20 m elevation level to depth. In addition, the developed vertical structures resulted from multiple intrusive events and relatively thick covered sedimentary strata should be the key inducements for the formation of the unique fluid downward migration in the Huangshaping deposit.

6. Conclusions

1. The pronounced lanthanide tetrad effect, high concentrations of Ga, Ta, Nb, U, Y, W and HREE but low concentrations of Ba, Sr, Eu and Zr in the hydrothermal K-feldspars indicate that strong water–rock interaction, with metasomatism occurring during the W–Mo ore-forming process.
2. Four samples of hydrothermal K-feldspar yielded precise $^{40}Ar/^{39}Ar$ plateau ages ranging from 152.9 ± 0.5 to 154.3 ± 0.6 Ma, recording the timing of potassic alteration event. These ages are younger than the mineralization ages of 154–160 Ma yielded by previous molybdenite Re–Os dating.
3. A downward fluid migration model is proposed for the Huangshaping polymetallic deposit, based on the $^{40}Ar/^{39}Ar$ and Re–Os geochronology. The mechanism of this migration can be ascribed to the gravity-driven fluid traveling along developed vertical structures under a fluid-overpressure condition.

Acknowledgements

This work was co-financed by the Fundamental Research Funds for the Central Universities, China University of Geosciences (Wuhan) (Grant No. CUG150612) and the National Natural Science Foundation of China (Grant No. 41502067). Prof. Hua Kong is acknowledged for his cooperation during the fieldwork. Helpful comments from anonymous reviewers and Prof. Franco Pirajno (Editor-in-Chief) improved and clarified the manuscript.

References

Boiron, M.C., Barakat, A., Cathelineau, M., Banks, D.A., Durisová, J., Morávek, P., 2001. Geometry and P-V–T–X conditions of microfissural ore fluid migration: the Mokrsko gold deposit (Bohemia). Chem. Geol. 173, 207–225.

Brockamp, O., Clauer, N., 2013. Hydrothermal and unexpected diagenetic alteration in Permian shales of the Lodève epigenetic U-deposit of southern France, traced by K-Ar illite and K-feldspar dating. Chem. Geol. 357, 18–28.

Chafe, A.N., Villa, I.M., Hanchar, J.M., Wirth, R., 2014. A re-examination of petrogenesis and $^{40}Ar/^{39}Ar$ systematics in the Chain of Ponds K-feldspar: "diffusion domain" archetype versus polyphase hygrochronology. Contrib. Miner. Petrol. 167, 1–17.

Chew, D.M., Flowerdew, M.J., Page, L.M., Crowley, Q.G., Daly, J.S., Cooper, M., Whitehouse, M.J., 2008. The tectonothermal evolution and provenance of the Tyrone Central Inlier, Ireland: Grampian imbrication of an outboard Laurentian microcontinent? J. Geol. Soc. Lond. 165, 675–685.

Chung, H.Y., Mungall, J.E., 2009. Physical constraints on the migration of immiscible fluids through partially molten silicates, with special reference to magmatic sulfide ores. Earth Planet. Sci. Lett. 286, 14–22.

Connolly, J.A.D., Podladchikov, Y.Y., 2004. Fluid flow in compressive tectonic settings: implications for midcrustal seismic reflectors and downward fluid migration. J. Geophys. Res. 109, B04201. http://dx.doi.org/10.1029/2003JB002822.

Deckart, K., Clark, A.H., Aguilar, C., Vargas, R., Bertens, A., Mortensen, J.K., Fanning, M., 2005. Magmatic and hydrothermal chronology of the giant Rio Blanco porphyry copper deposit, central Chile: implications of an integrated U-Pb and $^{40}Ar/^{39}Ar$ database. Econ. Geol. 100, 905–934.

Derome, D., Cathelineau, M., Lhomme, T., Curley, M., 2003. Fluid inclusion evidence of the differential migration of H_2 and O_2 in the McArthur River unconformity-type uranium deposit (Saskatchewan, Canada). Possible role on post-ore modifications of the host rocks. J. Geochem. Explor. 78–79, 525–530.

Ding, T., Ma, D.S., Lu, J.J., Zhang, R.Q., Zhang, S.T., 2016a. S, Pb, and Sr isotope geochemistry and genesis of Pb–Zn mineralization in the Huangshaping polymetallic ore deposit of southern Hunan Province, China. Ore Geol. Rev. 77, 117–132.

Ding, T., Ma, D.S., Lu, J.J., Zhang, R.Q., Zhang, S.T., Gao, S.Y., 2016b. Petrogenesis of Late Jurassic granitoids and relationship to polymetallic deposits in southern China: the Huangshaping example. Int. Geol. Rev. 58, 1646–1672.

Esser, R.P., Mcintosh, W.C., Heizler, M.T., Kyle, P.R., 1997. Excess argon in melt inclusions in zero-age anorthoclase feldspar from Mt. Erebus, Antarctica, as revealed by the $^{40}Ar/^{39}Ar$ method. Geochim. Cosmochim. Acta 61, 3789–3801.

Flude, S., Sherlock, S.C., Lee, M.R., Kelley, S.P., 2013. Disturbance to the $^{40}Ar/^{39}Ar$ system in feldspars by electron and ion beam irradiation. Chem. Geol. 355, 1–12.

Frank, M.R., Vaccaro, D.M., 2012. An experimental study of high temperature potassic alteration. Geochim. Cosmochim. Acta 83, 195–204.

Frazer, M., Whitaker, F., Hollis, C., 2014. Fluid expulsion from overpressured basins: implications for Pb-Zn mineralisation and dolomitisation of the East Midlands platform, northern England. Mar. Pet. Geol. 55, 68–86.
Harris, A.C., Dunlap, W.J., Reiners, P.W., Allen, C.M., Cooke, D.R., White, N.C., Campbell, I.H., Golding, S.D., 2008. Multimillion year thermal history of a porphyry copper deposit: application of U-Pb, $^{40}Ar/^{39}Ar$ and (U–Th)/He chronometers, Bajo de la Alumbrera copper-gold deposit, Argentina. Miner. Deposita 43, 295–314.
Hu, R.Z., Zhou, M.F., 2012. Multiple Mesozoic mineralization events in South China—an introduction to the thematic issue. Miner. Deposita 47, 579–588.
Kirkland, C.L., Daly, J.S., Chew, D.M., Page, L.M., 2008. The Finnmarkian Orogeny revisited: an isotopic investigation in eastern Finnmark, Arctic Norway. Tectonophysics 460, 158–177.
Lee, J.Y., Marti, K., Severinghaus, J.P., Kawamura, K., Yoo, H.S., Lee, J.B., Kim, J.S., 2006. A redetermination of the isotopic abundances of atmospheric Ar. Geochim. Cosmochim. Acta 70, 4507–4512.
Lei, Z.H., Chen, F.W., Chen, Z.H., Xu, Y.M., Gong, S.Q., Li, H.Q., Mei, Y.P., Qu, W.J., Wang, D.H., 2010. Petrogenetic and metallogenic age determination of the Huangshaping lead–zinc polymetallic deposit and its geological significance. Acta Geosci. Sin. 31, 532–540 (in Chinese with English abstract).
Leichmann, J., Jacher-Sliwczynska, K., Broska, I., 2009. Element mobility and fluid path ways during feldspar alteration: textural evidence from cathodoluminescence and electron microprobe study of an example from tonalities (High Tatra, Poland-Slowakia). Neues Jahrbuch für Mineralogie – Abhandlungen 186, 1–10.
Li, X.H., Li, W.X., Wang, X.C., Li, Q.L., Liu, Y., Tang, G.Q., 2009. Role of mantle-derived magma in genesis of early Yanshanian granites in the Nanling Range, South China: in situ zircon Hf–O isotopic constraints. Sci. China, Ser. D Earth Sci. 52, 1262–1278.
Li, H., Watanabe, K., Yonezu, K., 2014a. Zircon morphology, geochronology and trace element geochemistry of the granites from the Huangshaping polymetallic deposit, South China: implications for the magmatic evolution and mineralization processes. Ore Geol. Rev. 60, 14–35.
Li, H., Watanabe, K., Yonezu, K., 2014b. Geochemistry of A-type granites in the Huangshaping polymetallic deposit (South Hunan, China): implications for granite evolution and associated mineralization. J. Asian Earth Sci. 88, 149–167.
Li, X., Huang, C., Wang, C., Wang, L., 2016. Genesis of the Huangshaping W-Mo–Cu–Pb–Zn polymetallic deposit in Southeastern Hunan Province, China: constraints from fluid inclusions, trace elements, and isotopes. Ore Geol. Rev. 79, 1–25.
Lindsay, F.N., Herzog, G.F., Park, J., Delaney, J.S., Turrin, B.D., Swisher III, C.C., 2014. $^{40}Ar/^{39}Ar$ dating of microgram feldspar grains from the paired feldspathic achondrites GRA 06128 and 06129. Geochim. Cosmochim. Acta 129, 96–110.
Liu, W., 2002. Fluid–rock interaction during subsolidus microtextural development of alkali granite as exemplified by the Saertielieke pluton, Ulungur of the northern Xinjiang, China. Chem. Geol. 182, 473–482.
Ma, L.Y., Lu, Y.F., Qu, W.J., Fu, J.M., 2007. Re–Os isotopic chronology of molybdenites in Huangshaping lead–zinc deposit, southeast Hunan, and its geological implications. Miner. Deposits 26, 425–431 (in Chinese with English abstract).
Mao, J.W., Xie, G.Q., Guo, C.L., Chen, Y.C., 2007. Large-scale tungsten–tin mineralization in the Nanling region, South China: metallogenic ages and corresponding geodynamic process. Acta Petrol. Sin. 23, 2329–2338 (in Chinese with English abstract).
McDougall, I., Harrison, T.M., 1999. Geochronology and Thermochronology by the $^{40}Ar/^{39}Ar$ Method. Oxford University Press, New York.
McLaren, S., Dunlap, W.J., Powell, R., 2007. Understanding K-feldspar Ar/Ar data: reconciling models, methods and microtextures. J. Geol. Soc. Lond. 164, 941–944.
Pandit, D., 2015. Geochemistry of feldspar intergrowth microtextures from Paleoproterozoic granitoids in central India: implications to exsolution processes in granitic system. J. Geol. Soc. India 85, 163–182.
Plümper, O., Putnis, A., 2009. The complex hydrothermal history of granitic rocks: multiple feldspar replacement reactions under subsolidus conditions. J. Petrol. 50, 967–987.
Pujol, M., 2013. Argon isotopic composition of archaean atmosphere probes early earth geodynamics. Nature 498, 87–90.
Quan, T.J., Kong, H., Wang, G., Fei, L.D., Guo, B.Y., Zhao, Z.Q., 2012. Petrogenesis of the granites in the Huangshaping area: constrains from petrochemistry, zircon U-Pb chronology and Hf isotope. Geotec. Metall. 36, 597–606 (in Chinese with English abstract).
Reddy, S.M., Potts, G.J., Kelley, S.P., Arnaud, N.O., 1999. The effects of deformation-induced microstructures on intragrain $^{40}Ar/^{39}Ar$ ages in potassium feldspar. Geology 27, 363–366.
Reddy, S.M., Potts, G.J., Kelley, S.P., 2001. $^{40}Ar/^{39}Ar$ ages in deformed potassium feldspar: evidence of microstructural control on Ar isotope systematics. Contrib. Miner. Petrol. 141, 186–200.
Relvas, J.M.R.S., Barriga, F.J.A.S., Ferreira, A., Noiva, P.C., Pacheco, N., Barriga, G., 2006. Hydrothermal alteration and mineralization in the Neves-Corvo volcanic-hosted massive sulfide deposit, Portugal. I. Geology, mineralogy, and geochemistry. Econ. Geol. 101, 753–790.
Reynolds, P., Ravenhurst, C., Zentilli, M., Lindsay, D., 1998. High-precision $^{40}Ar/^{39}Ar$ dating of two consecutive hydrothermal events in the Chuquicamata porphyry copper system, Chile. Chem. Geol. 148, 45–60.
Sherlock, S.C., Lucks, T., Kelley, S.P., Barnicoat, A., 2005. A high resolution record of multiple diagenetic events: ultraviolet laser microprobe Ar/Ar analysis of zoned K-feldspar overgrowths. Earth Planet. Sci. Lett. 238, 329–341.
Solé, J., Cosca, M., Sharp, Z., Enrique, P., 2002. $^{40}Ar/^{39}Ar$ Geochronology and stable isotope geochemistry of Late-Hercynian intrusions from north-eastern Iberia with implications for argon loss in K-feldspar. Int. J. Earth Sci. 91, 865–881.
Streepey, M.M., Hall, C.M., van der Pluijm, B.A., 2002. The $^{40}Ar–^{39}Ar$ laser analysis of K-feldspar: constraints on the uplift history of the Grenville Province in Ontario and New York. J. Geophys. Res. 107. http://dx.doi.org/10.1029/2001JB001094.
Subias, I., Fanlo, I., Billstrom, K., 2015. Ore-forming timing of polymetallic-fluorite low temperature veins from Central Pyrenees: a Pb, Nd and Sr isotope perspective. Ore Geol. Rev. 70, 241–251.
Sun, S.S., McDonough, W.F., 1989. Chemical and isotopic systematics of oceanic basalts: implication for mantle composition and processes. Geol. Soc. Lond. Specl. Publ. 42, 313–345.
Tan, Q.P., Xia, Y., Xie, Z.J., Yan, J., 2015. Migration paths and precipitation mechanisms of ore-forming fluids at the Shuiyindong Carlin-type gold deposit, Guizhou, China. Ore Geol. Rev. 69, 140–156.
Taylor, S.R., McClennan, S.M., 1985. The Continental Crust: Its Composition and Evolution. Blackwell, Oxford, p. 312.
Wang, Z.L., Mao, J.W., Yang, J.M., Chen, W., Zhang, Z.H., 2004. $^{40}Ar–^{39}Ar$ age of K-feldspar from K-feldspar granite in the Qiaohuote copper deposit, Bayanbulak, Xinjiang, and its geological significance. Acta Geol. Sinica 78, 428–434.
Warnock, A.C., Zeitler, P.K., 1998. $^{40}Ar/^{39}Ar$ thermochronometry of K-feldspar from the KTB borehole, Germany. Earth Planet. Sci. Lett. 158, 67–79.
Wilson, N.S.F., Zentilli, M., Reynolds, P.H., Boric, R., 2003. Age of mineralization by basinal fluids at the El Soldado manto-type copper deposit, Chile: $^{40}Ar/^{39}Ar$ geochronology of K-feldspar. Chem. Geol. 197, 161–176.
Yao, J.M., Hua, R.M., Lin, J.F., 2005. Zircon LA–ICPMS U-Pb dating and geochemical characteristics of Huangshaping granite in southeast Hunan province, China. Acta Petrol. Sin. 21, 688–696 (in Chinese with English abstract).
Yao, J.M., Hua, R.M., Qu, W.J., Qi, H.W., Lin, J.F., Du, A.D., 2007. Re–Os isotope dating of molybdenites in the Huangshaping Pb–Zn–W–Mo polymetallic deposit, Hunan Province, South China and its geological significance. Sci. China, Ser. D Earth Sci. 50, 519–526.
Zhu, K.G., Yang, J.W., 2006. Numerical investigation of the influence of volcanic facies architecture on hydrothermal fluid migration: example of the Mount Read Volcanics, western Tasmania, Australia. J. Geochem. Explor. 89, 474–479.
Zhu, X.P., Li, G.M., Chen, H.A., Ma, D.F., Huang, H.X., 2015. Zircon U-Pb, molybdenite Re–Os and K-feldspar 40Ar/39Ar dating of the Bolong porphyry Cu–Au deposit, Tibet, China. Resour. Geol. 65, 122–135.